# Computational Rheology of Complex Fluids: Polymeric & Wormlike Micellar Solution Cases

J. Esteban López-Aguilar

## **ABSTRACT**

In this work, the essence of Non-Newtonian Fluid Mechanics and Computational Rheology is presented through three examples applied to the rheological characterisation of polymeric solutions using the SwanINNFM(q) family-of-fluids (1-5), and of worm-like micellar solutions using the BMP +  $_{\tau_p}$ rheological equation-of-state (6-8), within the computational modelling of two benchmark flows in Non-Newtonian Fluid Mechanics: contraction-expansion flow geometries and flow past a sphere. The predictive capabilities of our computational tools are demonstrated, where mathematical models derived from conservation principles are solved (9-11) alongside the construction of constitutive equations from theoretical rheology (1-11). These mathematical models are solved using a computational algorithm based on a hybrid formulation of spatial discretisation in the form of finite elements for the mass and momentum balance equations, and finite volumes for the constitutive equation (1-8, 12-15). In contraction-expansion type benchmark flows, firstly for polymeric fluids, experimental pressure-drop measurements were reproduced quantitatively using the SwanINNFM family-of-fluids (1-5). We were able, for the first time, to predict quantitatively and explain long-standing augmented excess pressure-drops and highly-dynamic vortex structures observed in the flow of polymeric Boger fluids (16-21). Building upon contraction-expansion flows of thixoviscoelastoplastic concentrated wormlike micellar solutions, the effects of

considering extreme shear thinning and flow segregation through yield stress and shear banding were demonstrated (6-8, 22). Using the BMP +  $_{\tau_p}$  constitutive model (8), shear bands are predicted in fully-developed flow zones away from the constriction, and their interaction with the complex deformation imposed by the contraction is reported. For the flow-past-sphere benchmark flow (7), numerical solutions obtained with the BMP +  $_{\tau_{D}}$  model qualitatively reproduce features reported experimentally for the descent of spheres in worm-like micellar solutions, i.e., a flow instability associated with oscillations in the sphere settling velocity and negative wakes (22), and, for relatively concentrated micellar solutions, asymmetrical yield fronts.

#### INTRODUCTION

One of the fundamental contributions of rheology is the identification of diverse materials as Newtonian (those that follow Newton's Law of Viscosity, i.e., those which display a constant viscosity at constant temperature and pressure), and as non-Newtonian, i.e., those that do not comply with the Newtonian definition. The latter manifest non-linear flow properties through a variable apparent viscosity with deformation rate, time of an imposed flow, and even displaying simultaneous liquid and solid properties in the form of viscoelasticity and yield stress, to name a few typical rheological responses (9-11).

In its practice, rheology divides its study into four main areas (9-11): (i) rheometry, which spans over material-property measurement, e.g., fundamentally

viscosity, elastic modulus, relaxation time; (ii) constitutive modelling, through which constitutive equations seek to reproduce and explain the material properties of complex fluids; (iii) non-Newtonian fluid mechanics, which studies the flow of non-Newtonian materials in complex geometries, whose essence lies in inhomogeneous deformations (deformations that combine shear and extension simultaneously in the flow field) and are reflected in physical arrangements with diverse geometric changes observed in nature and in technological applications, such as contractions and expansions, and flows around objects, among others; and (iv) computational rheology, which focuses its efforts in obtaining approximate numerical solutions to the flows studied in non-Newtonian fluid mechanics.

Complex fluids are materials with nonlinear rheological characteristics derived from their microstructure, which may be classified as soft matter (9-11). Complex fluids are found in countless technological applications, e.g., cements, paints, toothpaste, foams, crude oil and its heavy fractions, drilling muds in oil extraction, foodstuff, mayonnaise, plastics, reactive mixtures, and cosmetics (9-11, 22-31). In addition, many biological fluids, such as blood, mucus, saliva and tissues, may display non-linear rheological properties (32-36).

The combination of: (i) the non-linear rheological properties of complex fluids, (ii) the conservation equations, i.e. of mass, momentum and thermal energy, and (iii) the simultaneous non-homogeneous shear and extensional deformations imposed in complex flows, result

in mathematical problems of the highest complexity when attempting to describe, understand, and theoretically predict the experimental manifestations in non-Newtonian Fluid Mechanics (37-40). The interest of *Computational Rheology* is the prediction of complex flows of non-Newtonian materials. It bases its action on the development and application of advanced numerical techniques to the highly non-linear partial-differential-equation systems that represent flow problems whose solution is practically unattainable by exact methods (37-40).

There is a plethora of numerical algorithms for solving computational rheology problems (37-41). In general, their formulation has as a basis on Eulerian or Lagrangian frames of reference. The most popular Eulerian algorithms are based on finite-element and finite-volume methods (6-8, 37-40), devised to cover the mixed parabolic-hyperbolic nature of the mass-momentum-energy balance and constitutive equations. On the side of Lagrangian algorithms, particle dynamics methods (Smoothed Particle Hydrodynamics, Dissipative Particle Dynamics and lubrication dynamics methods), are among the most widely used (41), and represent a suitable option for the computational prediction of the rheology of suspensions and particulate systems (42).

Polymeric materials (melts and solutions) are made up of long-chain molecules, which interact closely through entanglement and reptation in molten and dissolved states. These interactions are the origin of their characteristic non-Newtonian features, in the form of marked shear thinning, and viscoelasticity through significantly-augmented normal-stress differences (10-11). The reflection of such rheological response in complex deformations has been a matter of extensive research (16-21). Studies on many benchmark flows have focused on their kinematic and dynamic response, for which augmented pressure drops and diverse vortex-enhancement mechanisms occupy a central role (16-21). In fact, the theoretical prediction and understanding of such features remain an open research topic to date, where efforts are still being concentrated in elucidating how polymeric materials respond under inhomogeneous deformations (1-6).

Wormlike micellar solutions (WLMs) are complex fluids composed of dispersions of elongated micelles that interact

essentially through relatively weak entanglements; these physical interactions promote their thixotropic, viscoelastic and plastic properties (22, 25-31). WLMs are also known as living polymers, due to their ability to restructure when flowing by two mechanisms, i.e., (i) reptation, as polymers do, and (ii) construction and destruction of micellar structures (22, 25-31). For these reasons and their varied rheological properties, these complex thixo-viscoelastoplastic materials are used in a wide range of applications, such as in cleaning and home and health-care products (shampoos, soaps, detergents, drug carriers); in the petroleum industry, as drilling and well-stimulation fluids; in pumping systems, lubricants and emulsifiers (22, 25-31).

The diversity of rheological properties of polymers and WLMs is a challenge for the development of constitutive equations capable of describing their experimental manifestations in simple and complex flows (37-40). Polymers and WLMs generally display shear thinning, extensional hardening and softening, viscoelasticity, thixotropy (16-21, 22, 25-31) and, in the specific case of WLMs, flow segregation in the form of yield stress (27) and banding (35). All of these responses occur simultaneously and manifest across diverse spatial-temporal scales (22, 25-31, 35).

Constitutive equations for polymeric materials are diverse and numerous, some coming from microscopic arguments and others based on continuum approaches (11). Among the most widely-used constitutive-equation approaches of differential nature are those of the FENE type, where the Peterlin and the Chilcott-Rallison closures dominate (11, 43-44), and the Phan-Thien-Tanner paradigm (45), which have been successful in reproducing and explaining the response of a wide range of polymer melts and solutions.

For WLMs, constitutive equations are still being developed (6-8, 22, 46-50). There are two main theoretical frameworks, namely, (i) theories based on structural variables, and (ii) microscopic theories. The former are the most popular, as they portray the evolution of the internal WLM structure, explicitly related to material functions (6-8, 46, 48-49). Among these models are those in the Bautista-Manero-Puig (BMP) (6-8) and de Souza-Mendes (48-49) families. The constitutive equations in the BMP framework predict

key properties of WLMs and other complex fluids, and have been successfully used to study the flow of WLMs in complex deformations (6-8). Microscopic theories study the interaction of micelles in their construction/destruction dynamics in flow, via kinetic equations whose solution is related to material properties through averages (47, 50).

Experimental studies on the flow of polymeric fluids and WLMs in complex geometries reveal rich features, with dynamic vortex-enhancement mechanisms and pressure drops. These act as alternative energy-dissipation mechanisms in contraction flows, and through drag coefficients in sphere settling, revealing instabilities manifested in particle oscillations and negative wakes (16-22, 51).

In benchmark contraction and contraction-expansion flows, complex vortex dynamics have been recorded experimentally. At low volumetric flow rates, symmetric kinematic structures are observed, similar to those observed in the contraction flow of Newtonian fluids. At high volumetric flow rate, asymmetric vortices, promoted by viscoelasticity, lead to time-dependent chaotic flows (16-22, 51).

In the sedimentation of smooth spheres in semi-dilute WLMs, oscillations in the particle descent velocity have been reported. These are caused by strong negative wakes behind the sphere; for polymeric liquids, a similar response is recorded as velocity overshoots (16-21, 51). These phenomena have been studied as flow instabilities with respect to the steady rate of descent characteristic of Newtonian fluids (22). In WLMs, these findings have been attributed to the complex dynamics of structure construction-destruction of the elongated micelles (leading to thixotropy) and the viscoelasticity of the micellar solution (6-8, 22). For concentrated mixtures, these thixo-viscoelastoplastic solutions form gels that display markedly-asymmetric yield fronts around the sphere (22, 51), as previously reported by Holenberg et al. (52) and Putz et al. (53).

One of the iconic manifestations of WLMs is a type of flow segregation called shear-banding, which is characterised by a spontaneous separation of the solution into two or more shear bands of material that coexist, supporting a constant shear stress, but with distinct apparent viscosity (8, 22, 35).

This paper presents a compendium of research work conducted by the author on computational predictions of the response of polymeric and WLM solutions in complex benchmark flows (1-8). These works illustrate the use of computational rheology in the numerical solution of two typical problems of non-Newtonian fluid mechanics: flows past a sphere (7), and flows through contractions and contraction-expansions (6,8). These benchmark flows have industrial and technological applicability; (i) flow around spheres is applied in particle suspension in medicine and the food industry (shelf life), and is also an approximation for clay transport in enhanced oil extraction fluids (37-40); whilst (ii) contraction-expansion flow is found in industrial equipment with pipe and fitting changes (37-40), and lies at the heart of polymer and food processing operations (22, 54).

# BALANCE AND CONSTITUTIVE EQUATIONS

The general statement of the problem of non-Newtonian flow in complex geometries, i.e., generalised flow systems with changes in shape and cross section, is based on the fundamental conservation equations and appropriate constitutive equations accounting for the rheological response of the materials considered. For incompressible, isothermal, non-Newtonian flow, the mass and momentum balance equations in dimensionless form are:

$$\nabla \cdot \boldsymbol{u} = 0, \tag{1}$$

$$Re\left(\frac{\partial \mathbf{u}}{\partial t} + \mathbf{u} \cdot \nabla \mathbf{u}\right) = -\nabla p + \nabla \cdot \mathbf{T},$$
 (2)

where u represents the velocity, p is the isotropic pressure, t symbolises time and  $\nabla$  is the gradient operator, which acts upon the three dimensions of space. The Reynolds number  $Re = \frac{\rho UL}{\eta_0}$  characterises the flow regime through the ratio of inertial forces experienced by the moving material against dissipative viscous forces. Here,  $\rho$  represents the material density,  $\eta_0 = \eta_{p0} + \eta_s$  is a characteristic viscosity, given by the level of the first Newtonian plateau in the flow curve (Fig. 1a), which is defined as the sum of the viscous contributions of the Newtonian solvent  $\eta_s$  and non-Newtonian solute  $\eta_{p0}$  at vanishing deformation rates, if the fluid is conceived as a solution. U and L represent, respectively,

characteristic velocity and length scales. Here, the characteristic velocity U is associated with the volumetric flow rate for flow around a sphere (Fig. 2a) and for a pressure-driven contraction flow (Fig. 2b); in contrast, U is associated with the velocity of the sliding wall of the contraction-expansion geometry in the modified Couette flow of Fig. 2c. Complementarily, the characteristic length L is related to the geometry considered: in the case of contraction-type flows, it is associated with the diameter of the constriction smallest gap, and, in the case of flow past a sphere, it is related to the particle diameter.

In non-Newtonian fluid mechanics, it is convenient to consider the fluids as solutions with solute and solvent components. This is a concept known as Elastic-Viscous Stress-Splitting (EVSS) (10-11), where the solvent is specified as Newtonian and the solute carries the

non-Newtonian characteristics of the solution. This approach allows for a broad applicability of rheological concepts to the characterisation of many types of materials with diverse non-Newtonian characteristics, such as polymer solutions (16-21), biofluids (32-36), metallic alloys (55), among many others. Thus, within the framework of the EVSS, the total stress tensor T is divided into two contributions: (i) the Newtonian solvent contribution, i.e.,  $\tau_s = 2\eta_s D = 2\eta_0 (1 - \beta)D$ ; and (ii) the contribution of the non-Newtonian solute  $\tau_p$ , for which a rheological equation-of-state must be specified and provides the nonlinear characteristics of the solution. Here,  $\mathbf{D} = \frac{1}{2} \left[ \nabla \mathbf{u} + (\nabla \mathbf{u})^T \right]$ is the rate-of-deformation tensor, which collects the symmetric shear and normal deformation rates that a fluid element can experience in a three-dimensional space. Furthermore, in the diffusive term on the

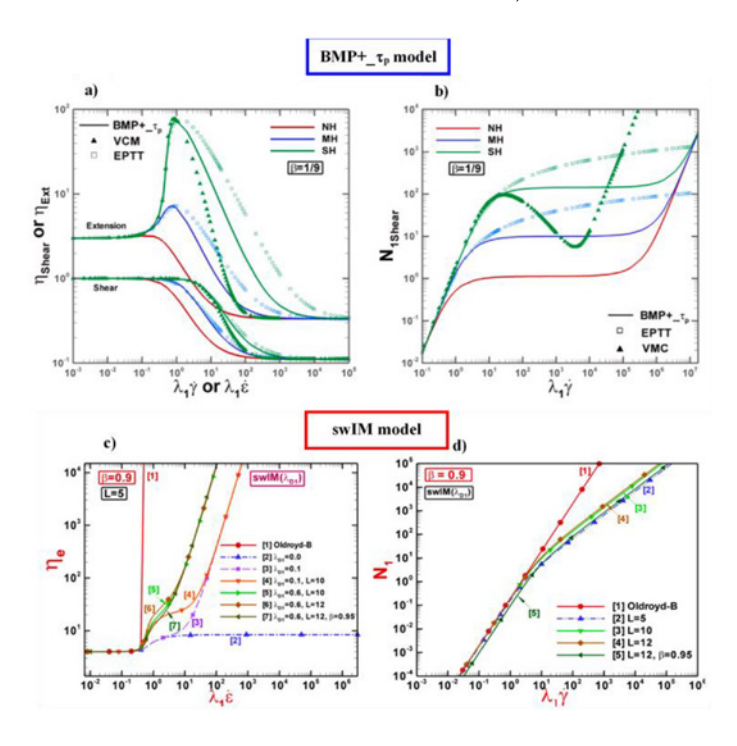


**FIGURE 1.** a) and b) BMP +  $_{-}$ τ $_{p}$  model material functions in steady simple shear and uniaxial extension; rheological responses for three fluids with apparently Null Hardening (NH;  $\{\omega,\xi_{Go}\}=\{4,1\}\}$ ), moderate (MH;  $\{\omega,\xi_{Go}\}=\{4,0.1125\}$ ) and severe (SH;  $\{\omega,\xi_{Go}\}=\{0.28,0.1125\}$ ) features;  $\beta=1/9$  - comparison against Exponential Phan-Thien-Tanner (EPTT) and Vasquez-Cook-McKinley (VCM) models. c) and d) SwanlNNFM(q) swlM model extensional viscosity and first normal-stress difference in shear. Reprinted from Journal of Non-Newtonian Fluid Mechanics, Vol. 309, J. Esteban López-Aguilar, Osvaldo Resendiz-Tolentino, Hamid R. Tamaddon-Jahromi, Marco Ellero, Octavio Manero, Flow past a sphere: Numerical predictions of thixo-viscoelastoplastic wormlike micellar solutions, 104902 1-22, Copyright (2022), and from Journal of Non-Newtonian Fluid Mechanics, Vol. 273, Michael F. Webster, Hamid R. Tamaddon-Jahromi, J. Esteban López-Aguilar, David M. Binding, Enhanced pressure drop, planar contraction flows and continuous spectrum models, 104184, Copyright (2019), with the permission of Elsevier.

RHS of the solvent stress equation, the solvent fraction  $\beta = \frac{\eta_s}{\eta_{p0} + \eta_s} = \frac{\eta_s}{\eta_0}$  defines a dimensionless viscosity by comparing the viscosity of the solvent  $\eta_s$  against the total viscosity of the solution at vanishing deformation rates  $\eta_0 = \eta_{p0} + \eta_s$ . The domain of this dimensionless viscosity is  $0 < \beta \le 1$ ; here,  $\beta = 1$  characterises a fluid with pure Newtonian characteristics and viscosity  $\eta_0$ , whilst, complementarily, the  $\beta \rightarrow 0$  limit defines the response of an extremely concentrated system with non-Newtonian features. Thus, the solvent fraction  $\beta$  serves as a measure of the viscous solute-to-solvent contributions to the total stress T.

To specify the rheological response of the non-Newtonian solute, whose stress is represented by  $\tau_p$ , and focusing on WLMs, this work considers the BMP theoretical framework in its most recent variant: the BMP +  $_{\rm T}_{\rm p}$  model (6-8). This rheological equation-of-state predicts the essential rheological response of WLMs (25-31). For this purpose, the solute stress obeys a generalised Oldroyd-B-type differential form:

$$f \boldsymbol{\tau}_p + De \overset{\nabla}{\boldsymbol{\tau}}_p = 2(1-\beta)\boldsymbol{D},$$
 (3)

where the Deborah number  $De = \lambda_1 \frac{U}{L}$  modulates the viscoelastic properties of the solution through the relaxation time of the material  $\lambda_1 = \frac{\eta_{p0}}{G_0}$ , which is defined by the ratio of the solute viscosity  $\eta_{p0}$  and the elastic modulus  $G_0$ , both measured at low deformation rates. The viscoelastic response of the solute resides in the upper-convected derivative of the stress:

$$egin{aligned} \stackrel{
abla}{m{ au}_p} &= rac{\partial m{ au}_p}{\partial t} + m{u} \cdot 
abla m{ au}_p - (
abla m{u})^T \cdot m{ au}_p - m{ au}_p \cdot 
abla m{u}. \end{aligned}$$

Its first term accounts for the variation of stress over time at a fixed point, the second term considers the temporal variation of stress due to motion, and the last two terms close the definition with the contribution given by the deformation of the material per se.

Finally, the first term on the LHS of Eq. (3) considers a material internal-structure functional  $f = \frac{\eta_{p0}}{\eta_p}$ , which, for models in the BMP formalism, is defined through a measure of the dimensionless solute fluidity. This internal-structure functional f obeys a temporal evolution through the following kinetic equation of fluid-structure construction and destruction (6-8):

$$\frac{\partial f}{\partial t} + \boldsymbol{u} \cdot \nabla f = \frac{1}{\omega} (1 - f) 
+ (\xi_{G_0} De - \xi f) | \boldsymbol{\tau}_p : \boldsymbol{D} |.$$
(5)

The LHS of Eq. (5) measures the spatialtemporal evolution of the dimensionless fluidity, whilst its RHS contains kinetic terms that measure the rates of internalstructure construction and destruction of the micellar solution, respectively, and which are reflected in the change of the fluidity of the material. Here, the dimensionless time  $\omega = \lambda_s \frac{U}{L}$  modulates the rate of formation of internal structure of the micellar solution. Complementarily,  $\xi_{G_0} = k_0 G_0 \frac{\eta_{p_0} + \eta_s}{\eta_{\infty} + \delta}$  and  $\xi = k_0 (\eta_{p_0} + \eta_s) \frac{U}{L}$  are dimensionless stresses associated with the destruction of the internal structure of the material; here,  $k_0$  is the inverse of the characteristic stress required to break the internal structure between the elongated micelles in suspension, and  $\eta_{\infty} + \delta$ is the viscosity of the solute at high deformation rates. The mechanism of structure destruction is promoted by the magnitude of the energy dissipated by the solute per unit volume  $|\tau_p:D|$  under flow. Furthermore, to include the formation of banded flows, the structure-destruction coefficient must take a linear functionality with respect to the rate-of-deformation tensor (8), i.e.,  $k(\mathbf{D}) = k_0 [1 + \vartheta II_{\mathbf{D}}]$ , where  $\vartheta$  is the shear-banding intensity parameter, and  $II_D = \sqrt{\frac{1}{2}D} : D$  is the second invariant of the rate-of-deformation tensor.

Eq. (5) stands for the latest model-variant in the BMP family, i.e., BMP +  $_{_{_{}}}\tau_{_{p}}$  model, which considers the coupling of thixotropy and viscoelasticity in the evolution of the material structure. Additionally, it provides a non-linear evolution of the first normal-stress difference in steady simple shear, and an extensional viscosity response with hardening and softening, all in line with fingerprints of typical WLMs (see Fig. 1a-b).

For polymeric solutions, the base constitutive equation approach used is that under the SwanINNFM(q) umbrella (1-5), which is constructed within a FENE-CR framework, and supplemented with a White-Metzner functionality on the viscous coefficient. Here, the conformation-tensor *A*-form of the base SwanINNFM(q) model is:

$$f(trA)(A-I) + De^{\nabla}A = 0.$$
 (6)

The FENE-CR structure functional is defined as:

$$f(tr\mathbf{A}) = \frac{1}{1 - \frac{tr\mathbf{A}}{L^2}},\tag{7}$$

where *L*<sup>2</sup> is the finite extensibility parameter. The Kramers rule translates the conformation tensor and the stress tensor signals as follows:

$$\boldsymbol{\tau}_{p} = \frac{1 - \boldsymbol{\beta}}{\boldsymbol{D}\boldsymbol{e}} f(tr\boldsymbol{A})(\boldsymbol{A} - \boldsymbol{I}). \tag{8}$$

Finally, the implementation of the dissipative extensional-function  $\phi(\dot{\varepsilon})=1+(\lambda_D\dot{\varepsilon})^2$  serves to devise an extensional viscosity boosting mechanism via an extension-dissipative timescale  $\lambda_D$  modulating the influence of the relevant extensional rate-of-deformation measure under specific complex flow and spatial geometry.  $\phi(\dot{\varepsilon})$  is defined as a quadratic form from the truncated Taylor-series approximation of the corresponding cosh-exponential functionality. This dissipative-extensional function  $\phi(\dot{\varepsilon})$  appears in the total stress equation as follows:

$$T = \frac{1 - \beta}{De} f(trA)(A - I)\phi(\dot{\varepsilon}) + 2\beta\phi(\dot{\varepsilon})D. \tag{9}$$

Multimode formulations and further functionalization have used on the viscous coefficient for specific applications - for further details, see (1-5). In Fig. 1c-d, typical response provided by the SwanINNFM(q) model variants, i.e., the swIM model, is illustrated. Here, one notes the control of the extensional viscosity response provided through  $\lambda_D$ , covering the window between the two limiting cases of FENE-CR and Oldroyd-B responses. In addition, these models provide a parametrisation for the first normal-stress difference in shear  $N_1$ , via a softening relative to the Oldroyd-B quadratic response.

# HYBRID NUMERICAL ALGORITHM OF FINITE ELEMENTS AND FINITE VOLUMES

The mathematical problem at hand in Eqs. (1)-(9), embodies a system of non-linear

partial differential equations that must be solved numerically with advanced algorithms. A hybrid numerical algorithm based on finite-element and finite-volume discretisation approximations is used in this work to obtain numerical solutions to the problem of polymeric and WLMs flow in complex geometries (1-8;12-15). This numerical algorithm is based on a hybrid scheme, built on a three-stage, semi-implicit, fractional-time scheme that utilises its finite-element discretisation for velocity and pressure, and its finite-volume approximation for stress and fluidity. This procedure combines the advantages and benefits offered by each discretisation approach individually. The Galerkin finite-element discretisation is applied to the components of the Cauchycontinuity equations [Eqs. (1)-(2)], with fractional steps for the momentum equation in Stage 1, the pressure-correction equation in Stage 2, and the incompressibility constraint in Stage 3, to ensure higher-order accuracy. Regarding its implementation, this leads to an elementby-element Jacobi iteration in space for Stages 1 and 3; whilst for pressure-correction in Stage 2, a direct Choleski solution method is used. Quadratic velocity interpolation is imposed on the triangular finite-element cell, along with linear interpolation for pressure. In contrast, for the finite-volume sub-cell, a triangular subdivision is constructed within the finite-element cell, by connecting the intermediate nodes of the triangular-cell. Here, stress and fluidity variables [Eqs. (3)-(8)] are located at the vertices of the finite-volume sub-cells; thus, interpolation of the solution is avoided. For further details, see (1-8; 12-15).

# **COMPLEX FLOW SETTINGS**

- 1) Contraction-expansion flow of polymeric solutions (1-5), and WLMs under shear-banding conditions (8).
  - In Fig. 2b, a schematic of a generalised flow domain for contraction flows is provided. Some boundary conditions are shared between the settings for the flow of polymeric liquids and WLMs. These are:
  - No-slip boundary conditions on solid walls. Velocity is imposed as Dirichlet boundary conditions on the contraction walls.
  - b. At the geometry inlet (left) and outlet (right), velocity and stress are imposed by solving the

- constitutive equation in simple shear flow.
- For the specific case of the flow of shear-banding WLMs (Fig. 2c):
- a) Flow inception. In this case, the flow is promoted through the drag exerted by the upper plate on the fluid. On the upper part of the geometry, the micellar solution moves with the plate velocity. In the lower part, the flow is fixed and anchored to the solid wall that forms the obstruction.
- b) Frame of reference. The geometry is a planar contraction-expansion, which we have designated as a modified Couette flow (8).
- c) Entry and exit conditions. Velocity may involve a single linear profile or a profile with two or more shear bands with different velocities but supporting a single stress level, characteristic of a banded flow. Pressure is readjusted by the obstacle and is maintained at a constant level in the fully-developed flow regions, as expected in a classical Couette flow.
- 2) Descent of a sphere in WLMs in a tube (7).
  - Fig. 2a illustrates the flow field of a sphere descending within a micellar fluid contained in a tube. For convenience, the geometry is shown horizontally. Since the system is symmetrical, half of the flow domain is shown, where the following boundary conditions apply:
  - a) No-slip boundary condition on the surface of the sphere. Here, the basic assumption of fluid adhesion on solid surfaces is considered as well, i.e., the velocity of the fluid in contact with the obstacle is equal to the sphere velocity.
  - b) Symmetry condition along the equatorial axis of the sphere. A symmetry condition is applied behind and in front of the sphere, where velocity and stress are continuous.
  - c) Flow inception. The flow in this computational arrangement is promoted by a constant velocity applied from left to right with respect to the orientation of the illustration, keeping the sphere fixed. Here, the imposed base

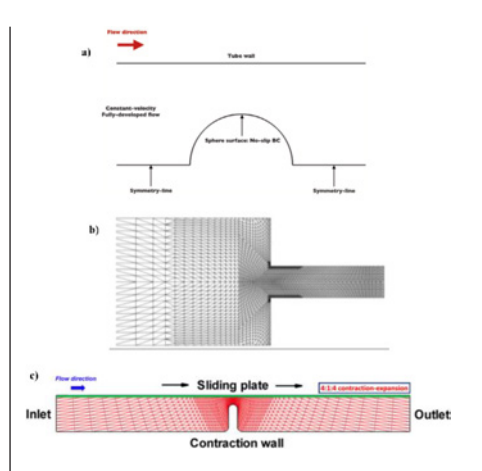


FIGURE 2. a) Schematics of flow past sphere; b) Schematics of 4:1 contractionexpansion flow; and c) Schematics of the flow through a plane contraction-expansion with rounded edges. Reprinted from Journal of Non-Newtonian Fluid Mechanics, Vol. 309, J. Esteban López-Aguilar, Osvaldo Resendiz-Tolentino, Hamid R. Tamaddon-Jahromi, Marco Ellero, Octavio Manero, Flow past a sphere: Numerical predictions of thixo-viscoelastoplastic wormlike micellar solutions, 104902 1-22, Copyright (2022), with permission from Elsevier, from Physics of Fluids, Vol. 28, J. Esteban López-Aguilar, Hamid R. Tamaddon-Jahromi, Michael F. Webster, Ken Walters. Numerical vs experimental pressure drops for Boger fluids in sharp-corner contraction flow, 103104-23, Copyright (2016), and from Vol. 35, J. Esteban López-Aguilar, Hamid R. Tamaddon-Jahromi, Marco Ellero, Octavio Manero, Shear banding predictions for wormlike micellar systems under a contraction-expansion complex flow, 063101 1-22, Copyright (2023), with permission from AIP Publishing.

volumetric flow rate is unitary, which is increased consecutively in the simulations. This increase in flow rate is reflected through the increase in Deborah number, which, in this case, correlates with the volumetric flow rate as follows:  $De = \lambda_1 \frac{U}{L}$ , where U is the approaching velocity (Fig. 2a).

For the three examples treated in this work, the following implementations are considered for numerical stability and convergence:

a) The VGR correction. Nonhomogeneous extensional

deformations are specified through the relevant velocitygradient components in the symmetry lines - this is referred to in (6-8) as the VGR correction. The ABS-f correction. The socalled ABS-f correction is considered, where an absolute value operation is applied to the flow quantities used in the internal-structure *f*-functional within the constitutive equation promoting the exposure of non-linear rheological features of the material. This correction provides material function prediction (in these cases, viscosity) in line with the Second Law of Thermodynamics (6-8). For the BMP +  $_{\tau_p}$  model, the ABS-fcorrection applies over the dissipation function  $| \boldsymbol{\tau}_p : \boldsymbol{D} |$  components in Eq. (5), whilst in the SwanINNFM(q) models, this correction is implemented over the trA-components.

# RESULTS

In this section, the main results of modelling the flows described in the previous section through the SwanINNFM(q) and BMP +  $_{}$   $_{}$   $_{}$  equations are described, for which numerical solutions were obtained using our hybrid finite-element/finite-volume numerical algorithm (1-8;12-15).

For flow past a sphere (7), the predictive capabilities of our numerical tools are described in terms of: (i) the dimensionless drag coefficient  $\frac{K}{K_{Newtonian}}$ , which reflects the energy required for a sphere to descend in a WLMs and reveals flow transitions; (ii) vortex dynamics, where the spatial evolution of the flow field behind the sphere is studied and a nonhomogeneous uniaxial extensional flow is verified, i.e., with an inhomogeneous uniaxial extension rate; and (iii) the correlation of this response with the evolution of the internal structure parameter of the material f. For the flow through contraction-expansion geometries, similar signals are gathered for polymeric liquids, where significantly-augmented pressure drops and highly-dynamic vortex structures are recorded, whilst for a WLMs capable of developing shear bands (8), the results reflect: (i) velocity fields with two or more flow bands and the interaction of this structured flow with the obstruction; (ii) with this, the characteristics of a banded flow are studied in a two-dimensional geometry and their consequences on other variables, such as dimensionless fluidity and normal stresses (viscoelasticity).

# 1. Contraction-expansion flow of polymeric solutions (1-5)

In Fig. 3, a comparison between experimental and predictive trends on pressure drops against flow rate increase is provided for a sharp-cornered axisymmetric 4:1 contraction flow of Boger PAA/ corn syrup based fluids (1). Here, the experimental viscoelastic pressure-drop augmented trends are matched quantitatively with our SwanINNFM(q) model under  $\lambda_D = 1.2$ . In addition, kinematic information accompanies these trends, with a vortex-enhancement path starting with a salient-corner vortex at relatively small flow rates that grows in size and intensity with Q-rise, evolving into an elastic-corner vortex that dominates the constriction. Moreover, vortex-intensity  $-\Psi_{min}$  follows a monotonic rising trend with Q-rise. This may be correlated with the basic SwanINNFM(q) extensionalviscosity  $\eta_{Ext}$ -response, for which  $\lambda_D \neq 0$ promotes a sustained rise (see Fig. 1c).

In Fig. 4, excess pressure drop (*epd*) against dimensionless flow rate data is provided for the flow of a similar Boger PAA/corn syrup fluid in a sharp-cornered 10:1:10 axisymmetric contraction-expansion geometry (2). Outstanding *epd* values were experimentally recorded, with the largest signal levelling over some five-to-six times that

of an equivalently-viscous Newtonian corn-syrup fluid. Here, the swIM modelvariant in the SwanINNFM(q) familyof-fluids captures the whole window of *epd*-response under rising  $\lambda_D$ . A sample of the vortex activity for these fluids is provided in Fig. 5, where, under the same 10:1:10 contraction flow settings and an average  $\lambda_D = 0.3$ , renders a map of the vortex-enhancement path predicted. Here, a three-staged vortex evolution with De-rise is recorded, with a symmetric salient-corner vortex regime at relatively small dimensionless flow rates, followed by the coexistence of salient-corner and lip vortices at intermediate De-numbers, to finally evolve into an elastic-corner-vortex regime at large

In Fig. 6, attention is paid to a distinct contraction flow setting under 4:1 planar sharp-cornered configuration, in which we were able to capture the so-called bulb flow reported by Binding and Walters (21). Here, we provide a vortex-activity path that resembles the qualitative description provided by Binding and Walters (21), for which, after a steady regime dominated by relatively reduced salient-corner vortices, a lip vortex arises with Q-rise in a transitionary regime, which strengthens and coexists with the salient-corner structure, thus creating the bulb flow. This transitionary phase is characterised computationally by solution fluctuation, recorded through periodic variations of pressure, velocity and stress, illustrated here through their L2-norms.

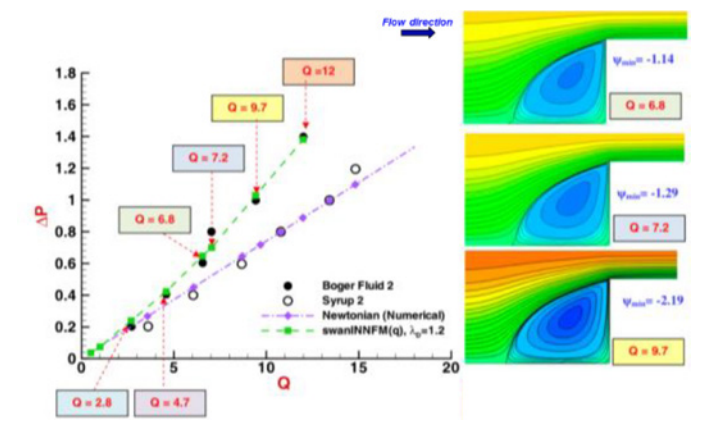


**FIGURE 3.** Pressure drops against flow rate, vortex intensity and streamlines; SwanlNNFM(q) swlM model-variant,  $\lambda_d = 1.2$ . Reprinted from Physics of Fluids, Vol. 28, J. Esteban López-Aguilar, Hamid R. Tamaddon-Jahromi, Michael F. Webster, Ken Walters. Numerical vs experimental pressure drops for Boger fluids in sharp-corner contraction flow, 103104–23, Copyright (2016), with the permission of AIP Publishing.

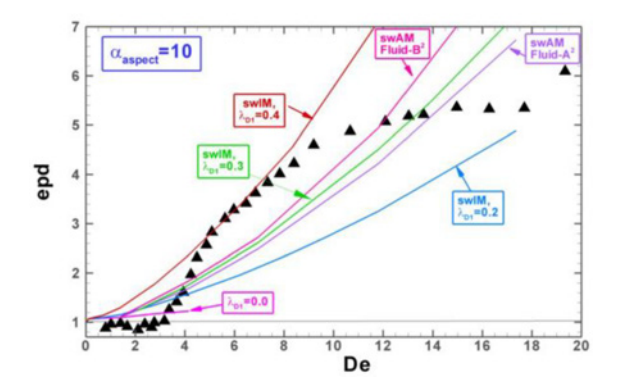


**FIGURE 4.** Excess pressure drop against dimensionless flow rate; SwanlNNFM(q) swlM and swAM model-variant; 10:1:10 sharp-cornered axisymmetric contraction-expansion. Reprinted from Physics of Fluids, Vol. 29, J. Esteban López-Aguilar, Michael F. Webster, Hamid R. Tamaddon-Jahromi, Octavio Manero, David M. Binding, Ken Walters, On the use of continuous spectrum and discrete-mode differential models to predict contraction-flow pressure drops for Boger fluids., 121613–18, Copyright (2017), with the permission of AIP Publishing.

These kinds of trends in augmented pressure drops and vortex-enhancement mechanism are found with different flow settings and under varying constriction aspect ratios. In general, the outlined pressure-drop-against-flow-rate trends are correlated with the extensional viscosity features of the polymeric solution studied. Vortex structure and evolution have been found correlated with the first normal-stress response within the corners of the constriction. For further details on these general findings, the characteristics of the constitutive models used, and the numerical implementation, the author refers the reader to (1-5).

#### 2. Flow past sphere of WLMs (7)

In Fig. 7, predictions obtained for the dimensionless drag coefficient  $\frac{K}{K_{Newtonian}}$ are plotted against dimensionless volumetric flow rate in the form of Deborah number De, for three semi-dilute WLMs under a solvent fraction of  $\beta = 0.5$  and three variations of extensional properties with extensional response apparently No-Hardening (NH), Moderate Hardening (MH) and Strong Hardening (SH) - see Fig. 1a and its extensional viscosity response. The results obtained for  $\frac{K}{K_{Newtonian}}$  are referred to the ideal case of a Newtonian fluid with equivalent viscosity; this base case is plotted in Fig. 7 and appears as a unitary horizontal line. The WLMs under NH shows a stronger and abrupt decline with De-rise, even showing a plateau at high De-levels that asymptotes to  $\frac{K}{K_{Newtonian}} = 0.5$ . The MH

case reflects a similar decrease, although its  $\frac{K}{K_{Newtonian}}$  values are higher than those under the NH case. This response correlates with the relatively higher forces and viscosities, both in shear and extension, sustained by the MH solution (Fig. 1a-b), a trend that is sustained and is even more marked with the SH case. Interestingly, these declining  $\frac{K}{K_{Newtonian}}$ -trends are observed in typical experimental studies of sphere settling in WLMs (22).

With focus on the MH case in Fig. 7, it is worth highlighting the fluctuations recorded in  $\frac{K}{K_{Newtonian}}$  at high De. These fluctuations are associated with the development of vortices behind the sphere, which are one of the key flow structures in flow past spheres, i.e., the development of negative wakes (see Fig .8a). These flow instabilities are characterised by occurring at relatively high De; for the case illustrated in Fig. 7, the critical dimensionless volumetric flow rate for the instability is  $De_{crit} = 24$ . Here in Fig. 8a, one can see a sample of the vortex located at the equator of the sphere, which forms, grows, intensifies and suppresses cyclically over time (see (7)). It is worth mentioning that this type of instabilities have been widely studied experimentally, happening at De numbers in the range of tenths of units (22, 51). Our research group is one of the first to report the theoretical-computational description of this phenomenon for WLMs (7).

In Fig. 8b, the dimensionless fluidity is illustrated, where a fluctuating state is apparent as a reflection of the vortex

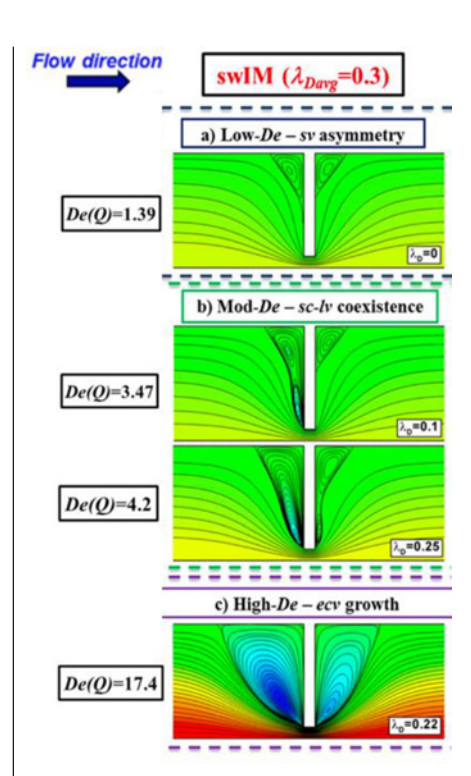
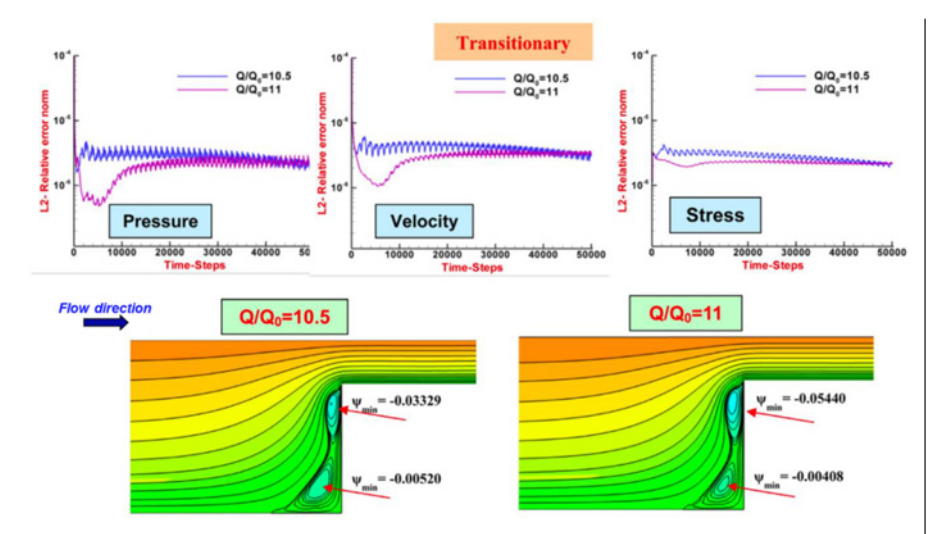


FIGURE 5. Streamlines against flow rate; SwanlNNFM(q) swlM model-variant; 10:1:10 sharp-cornered axisymmetric contraction-expansion. Reprinted from Physics of Fluids, Vol. 29, J. Esteban López-Aguilar, Michael F. Webster, Hamid R. Tamaddon-Jahromi, Octavio Manero, David M. Binding, Ken Walters, On the use of continuous spectrum and discrete-mode differential models to predict contraction-flow pressure drops for Boger fluids., 121613–18, Copyright (2017), with the permission of AIP Publishing.

activity and the associated negativewake cycle of Fig. 8a. One should recall that this dimensionless fluidity serves, in the BMP +  $_{\tau_p}$  model, to estimate the level and the evolution of the material internal structure. Thus, these graphs depict, by correspondence, the change in the structure of the material due to the deformation imposed by the obstacle. In this case, it is worth highlighting that, in the instance of fluctuations in the sphere settling velocity, the structure of the material behind the sphere shows significant variation, revealing the influence of the predominantly-extensional inhomogeneous flow in the obstacle wake. This phenomenon has been attributed as the ruling factor for the development of fluctuations in the sphere settling velocity in WLMs, associated with a mechanism of micellar sudden rupture in the sphere

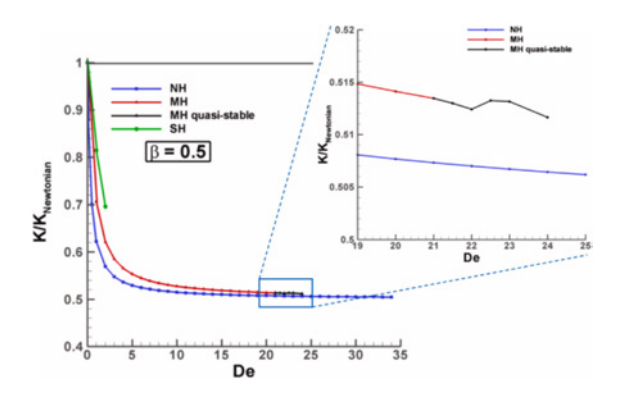


**FIGURE 6.** Streamlines and L2-norms. Bulb flow. SwanlNNFM(q) swAM model-variant. Reprinted from Journal of Non-Newtonian Fluid Mechanics, Vol. 273, Michael F. Webster, Hamid R. Tamaddon-Jahromi, J. Esteban López-Aguilar, David M. Binding, Enhanced pressure drop, planar contraction flows and continuous spectrum models, 104184, Copyright (2019), with the permission of Elsevier.

wake due to the stretching they suffer (22, 51).

Moving on to the analysis of *concentrated WLMs*, characterised with the BMP +  $_{}$ T $_{p}$  model, under  $\beta \rightarrow 0$ , one should recognise that these materials take a semi-solid consistency, where their plastic properties are measured through an apparent yield stress. Numerical predictions are illustrated in Fig. 9 through yield-front data. These yield fronts contrast the yielded zones (fluidised; in red) close to the sphere and the unyielded zones (semi-solid; in blue). These regions

are identified via the comparison of the stress experienced by the fluid, measured through the stress second invariant experienced by the solute, i.e.,  $II_{\bar{\tau}_p} = \sqrt{\frac{1}{2}} \overline{\bar{\tau}_p} : \overline{\bar{\tau}_p}$ , and the yield stress  $\tau_0$ . In Fig. 9, graphical evidence is provided contrasting the effects of decreasing the solvent fraction  $\beta$  (increasing plasticity and thus  $\tau_0$ ) in the range  $0.005 \le \beta \le 1/9$ , against De. Here, one may note that, under a fixed De, decreasing  $\beta$  promotes the growth of the semisolid blues zones, even finding instances where there is practically no liquefied material in the flow field;



# 3. Shear Banding in Complex Deformations (8)

In this subsection, the flow of a WLM susceptible to forming shear bands is analysed, i.e., in viscosity. The flow curves and material properties of WLMs that can develop banded flows are illustrated in Fig. 10. Here, the key feature for developing shear bands is the presence of a total shear-stress  $T_{xy}$  flow curve following a non-monotonic trend (Fig. 10a): a sigmoidal curve with a negativelysloped section in an intermediate shearrate range. This region of the flow curve is identified as the unstable branch, whilst the sections with positive slope at high and low shear rates are designated as stable branches. In Fig. 10b, the reflection of the development of shear bands can be observed: the presence of the unstable zone in the stress causes an exaggerated shear thinning in the WLMs apparent viscosity, alongside the development of non-monotonic curves in the first normalstress difference in shear  $N_{1_{Shear}}$  (Fig. 10c); the extensional viscosity remains invariant. The development of banded flows is promoted in the BMP+  $_{-}\tau_{_{\! P}}$  model through increasing the dimensionless shear-banding intensity parameter  $\zeta = \vartheta \frac{U}{L}$ , which in Fig. 10 takes the values of  $\zeta = \{0,3\}$ . Here, the  $\zeta = 0$  case represents a fluid without the ability to develop shear bands (note its monotonic curve), whilst  $\zeta = 3$  characterises a fluid with an unstable branch at intermediate shear rates, capable of developing shear bands. Other models, such as the Vasquez-Cook-McKinley (VCM) model, produce similar responses (50), as depicted in Fig. 10.

In Fig. 11, numerical solutions are provided of the modified Couette flow of a banding WLM fluid under  $\zeta = 3$  and a non-banding fluid under  $\zeta = 0$ . Here, under the banding mode (left), the development of two shear bands in  $U_x$  is observed in the fully-developed flow

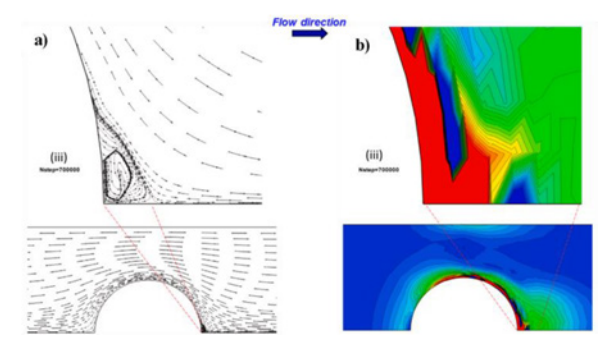


**FIGURE 8.** a) Stream function and b) dimensionless fluidity at  $De_{crit} = 24$ ; BMP +  $\_\tau_p$  model; MH:  $\{\omega, \xi_{GO}\} = \{4,0.1125\}$ ;  $\beta = 0.5$ . Development of negative wakes. Reprinted from Journal of Non-Newtonian Fluid Mechanics, Vol. 309, J. Esteban López-Aguilar, Osvaldo Resendiz-Tolentino, Hamid R. Tamaddon-Jahromi, Marco Ellero, Octavio Manero, Flow past a sphere: Numerical predictions of thixo-viscoelastoplastic wormlike micellar solutions, 104902 1-22, Copyright (2022), with permission from Elsevier.

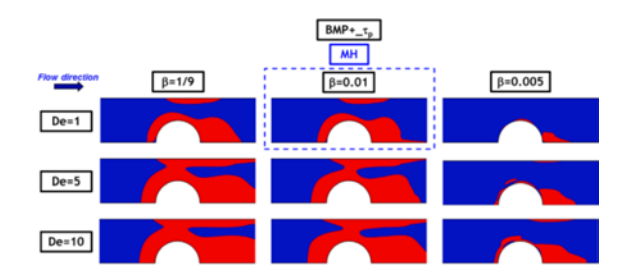


**FIGURE 9.** Yield fronts against flow rate and solvent fraction; BMP +  $_{\tau_p}$  model; MH:  $\{\omega,\xi_{G0}\}=\{4,0.1125\}$ ;  $\beta=\{1/9,0.01,0.001\}$ . Reprinted from Journal of Non-Newtonian Fluid Mechanics, Vol. 309, J. Esteban López-Aguilar, Osvaldo Resendiz-Tolentino, Hamid R. Tamaddon-Jahromi, Marco Ellero, Octavio Manero, Flow past a sphere: Numerical predictions of thixo-viscoelastoplastic wormlike micellar solutions, 104902 1-22, Copyright (2022), with permission from Elsevier.

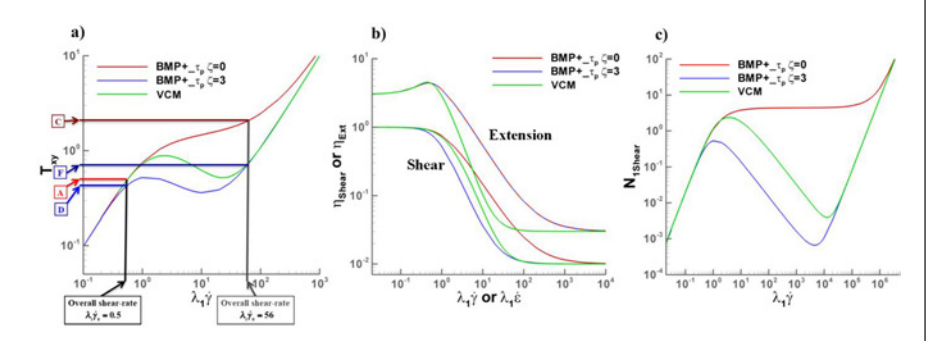


**FIGURE 10.** (a) Shear stress  $T_{xy}$ , (b) shear  $\eta_{Shear}$  and extensional  $\eta_{Ext}$  viscosities, and (c) first normal-stress difference in shear  $N_{1_{Shear}}$ ; BMP + \_ $\tau_p$  model; { $\omega, \xi_{GO}$ } = {4,0.1136},  $\beta$  = 0.01,  $\zeta$  = {0,3}. Reprinted from Physics of Fluids, Vol. 35, J. Esteban López-Aguilar, Hamid R. Tamaddon-Jahromi, Marco Ellero, Octavio Manero, Shear banding predictions for wormlike micellar systems under a contraction–expansion complex flow, 063101 1-22, Copyright (2023), with permission from AIP Publishing.

regions far from the constriction, one with red shading, which correlates with relatively high velocities, and another with blue shading, which corresponds to relatively lower velocities. This response is translated in the shear-rate  $\frac{\partial U_x}{\partial y}$  plot into two bands marked by relatively high (red) and low (blue) shear rates, which occupy the flow domain, and coincide with the viscosity, fluidity and normal-stress  $T_{xx}$ bands, respectively. In contrast, the shearstress  $T_{xy}$  and pressure P fields remain homogeneous in the fully-developed flow regions; the small fluctuations in  $T_{xy}$  are related to the discontinuity posed by the interface between the two shear bands and are minimal in magnitude.

Regarding the phenomenology observed in the contraction zone, one notes that the fully-developed banded flow developed by the fluid under  $\zeta=3$  is lost when the material interacts with the obstacle. Once the material leaves the constriction zone and advances towards the simple-shear, fully-developed-flow downstream region, the material develops shear bands again.

One can contrast the behaviour of a WLM fluid not susceptible to developing shear bands, i.e., under non-banding  $\zeta=0$  mode in Fig. 11 (right). Here, the flow structure contrasts with what was described for the banding case, since the flow fields do not display abrupt changes in the form of bands, although asymmetry is maintained, promoted by the thixoviscoelastic BMP +  $_{\tau_p}$  properties.

It is worth mentioning that this is one of the first theoretical-computational works capable of reproducing a shear-banded flow in a geometry that combines shear and extensional flows simultaneously (8). In addition, these predictions can be used to analyse the flow of other types of complex fluids that are processed in extruders, by idealising the contraction that materials undergo in nozzles to acquire their final shape, such as molten polymers and foods (54).

# CONCLUSIONS

In this work, the area of action of Non-Newtonian Fluid Mechanics and Computational Rheology has been fundamentally explained (9-11, 37-40), and its predictive potential for problems related to its application has been illustrated through three examples applied to a variety of materials widely used in the chemical industry: polymeric (16-21) and

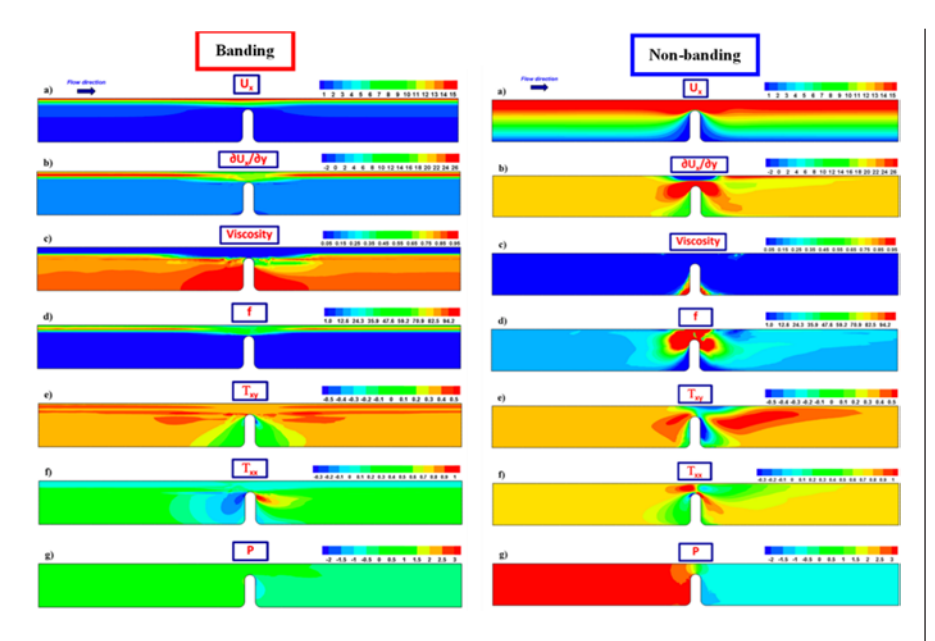


**FIGURE 11.** Velocity in the *x*-direction  $v_x$ , shear rate  $\frac{\partial v_x}{\partial y}$ , viscosity  $\eta_p$ , fluidity  $f = \frac{\eta_{p0}}{\eta_0}$ , shear stress  $T_{xy}$ , normal stress in *x*-direction  $T_{xx}$ , pressure P; BMP + \_ $\tau_p$  model;  $\zeta = \{0,3\}$ ,  $\{\omega,\xi_{G0}\} = \{4,0.1136\}$ ,  $\beta = 0.01$ . Reprinted from Physics of Fluids, Vol. 35, J. Esteban López-Aguilar, Hamid R. Tamaddon-Jahromi, Marco Ellero, Octavio Manero, Shear banding predictions for wormlike micellar systems under a contraction–expansion complex flow, 063101 1-22, Copyright (2023), with permission from AIP Publishing.

wormlike micellar solutions (22, 26-31). The examples discussed in this article are benchmark flows in Non-Newtonian Fluid Mechanics (22, 37-40): (i) flow past a sphere and (ii) flow through diverse contraction-expansion settings. The constitutive equations used to characterise the viscoelastic and thixo-viscoelastoplastic rheological properties of polymeric and WLMs are the SwanINNFM(q) model (1-5) and the BMP +  $_{\rm T_p}$  model (6-8). The mathematical models resulting from the consideration of the isothermal twodimensional flow under incompressible conditions of polymeric and WLMs are solved with a hybrid finite element-volume numerical algorithm (1-8, 12-15).

With these theoretical and numerical tool-sets, we reported success in the prediction of key experimental signals in contraction-type flows of polymeric solutions, such as augmented pressure-drops with respect to Newtonian fluids, and complex vortex-enhancement routes that reveal dissipation mechanisms enabling the flow of these materials through constricted geometries (1-5), even capturing shear-banded flows in planar contraction-expansion flow-settings for WLMs (7). Computational signals for instabilities in particle settling within dilute WLMs were reported, for which fluctuations in the

flow field behind the sphere are recorded through cyclical-growing vortices and highly-variable fluid structure (8). For more concentrated WLMs, asymmetrical yield fronts were captured, resembling experimental flow structures reported for Carbopol and typical WLMs (8).

Through the description of these three examples, the usefulness that theoretical-computational predictive tools can have for non-Newtonian fluid mechanics is demonstrated, where the detailed computational solution of complex flow systems with non-Newtonian materials provides numerical data that can help to model, describe, analyse, and understand flow processes of interest in industrial and technological applications for other various materials, such as metallic alloys (55), in medicine, and in bioengineering (33-37).

#### **ACKNOWLEDGEMENTS**

The author acknowledges the support from Secretaría de Ciencia, Humanidades, Tecnologías e Innovación (SECIHTI – Ex-CONAHCYT, México - grant number CF-2023-I-318), from Universidad Nacional Autónoma de México (UNAM) (grant numbers PAPIIT IN106424, PAPIME PE103125 y PAIP 5000-9172 Facultad de Química).

# **Author**



J. Esteban López-Aguilar is a Professor of Chemical Engineering at the Chemical Engineering Department, Facultad de Química, Universidad Nacional

Autónoma de México (UNAM) since 2017. He received his Bachelors (2007) and Masters (2009) degrees from UNAM, and his PhD in Chemical Engineering (2016) from Swansea University (UK), where he also carried out postdoctoral activities at the Zienkiewicz Centre for Computational Engineering (2016-2017). He is Level 1 in the National System of Researchers, SECIHTI, MX-Government. Esteban belongs to various scientific societies, including his Associate Membership to the Institute of Non-Newtonian Fluid Mechanics (UK), Visiting Fellowship to the Basque Centre for Applied Mathematics (BCAM; Bilbao, Spain), and Board Membership to the Mexican Polymer Society. His research interests focus on Non-Newtonian Fluid Mechanics, with special emphasis on computational rheology and constitutive modeling of complex fluids and soft matter, such as viscoelastic surfactant solutions, melts and polymer solutions, suspensions and biofluids.

### REFERENCES

- López-Aguilar, J. E., Tamaddon-Jahromi, H. R., Webster, M. F., Walters, K. (2016) Numerical vs experimental pressure drops for Boger fluids in sharp-corner contraction flow, Phys. Fluids 28, 103104 10.1063/1.4966022.
- 2. López-Aguilar, J. E., Webster, M. F., Tamaddon-Jahromi, H. R., Pérez-Camacho, M., Manero, O. (2016) Contraction-ratio variation and prediction of large experimental pressure-drops in sharp-corner circular contraction-expansions-Boger fluids, J. Non-Newton. Fluid Mech. 237, 39–53 10.1016/j.jnnfm.2016.10.005.
- 3. López-Aguilar, J. E., Webster, M. F., Tamaddon-Jahromi, H. R., Manero, O., Binding, D. M., Walters, K. (2017) On the use of continuous spectrum and discrete-mode differential models to predict contraction-flow pressure drops for Boger fluids, Phys. Fluids, 29, 121613–18 10.1063/1.4991872.
- Webster, M. F., Tamaddon-Jahromi, H. R., López-Aguilar, J. E., Binding, D. M. (2019) Enhanced pressure drop, planar contraction flows and continuous spectrum models, J. Non-Newton. Fluid Mech. 273, 104184 10.1016/j.jnnfm.2019.104184.

- 5. López-Aguilar, J. E., Tamaddon-Jahromi, H. R. (2020) Computational Predictions for Boger Fluids and Circular Contraction Flow under Various Aspect Ratios, Fluids 5, 85–22 10.3390/fluids5020085.
- López-Aguilar, J. E., Webster, M. F., Tamaddon-Jahromi, H. R., Manero, O. (2018) Predictions for circular contraction-expansion flows with viscoelastoplastic & thixotropic fluids, J. Non-Newton. Fluid Mech. 261, 188–210 10.1016/j.jnnfm.2018.09.001.
- López-Águilar, J. E., Resendiz-Tolentino, O., Tamaddon-Jarohmi, H. R., Ellero, M., Manero, O. (2022) Flow past a sphere: Numerical predictions of thixo-viscoelastoplastic wormlike micellar solutions, J. Non-Newton. Fluid Mech. 309, 104902 10.1016/j.jnnfm.2022.104902.
- 8. López-Aguilar, J. E., Tamaddon-Jahromi, H. R., Manero, O. (2023) Shear banding predictions for wormlike micellar systems under a contraction–expansion complex flow, Phys. Fluids **35**, 063101 10.1063/5.0143432.
- 9. Bird, R. B., Stewart, W. E., Lightfoot, E. N. (1960) Transport Phenomena, Wiley: 1st Edition.
- Barnes, H. A., Hutton, J. F., Walters, K. (1989) An introduction to rheology, Elsevier: 1st Edition.
- 11. Bird, R. B., Armstrong, R. C., Hassager, O. (1987) Dynamics of Polymeric Liquids, John Wiley & Sons: 1st Edition.
- 12. Matallah, H., Townsend, P., Webster, M. F. (1998) Recovery and stress-splitting schemes for viscoelastic flows, J. Non-Newton. Fluid Mech. **75**, 139–166 10.1016/S0377-0257(97)00085-2.
- Wapperom, P., Webster, M. F. (1998) A second-order hybrid finite-element/ volume method for viscoelastic flows, J. Non-Newton. Fluid Mech. 79, 405–431 10.1016/S0377-0257(98)00124-4.
- Webster, M. F., Tamaddon-Jahromi, H. R., Aboubacar, M. (2005) Time-dependent algorithms for viscoelastic flow: Finite element/volume schemes, Numer. Meth. Partial Differ. Equ. 21, 272–296 10.1002/ num.20037.
- 15. Belblidia, F., Matallah, H., Webster, M. F. (2008) Alternative subcell discretisations for viscoelastic flow: velocity-gradient approximation, J. Non-Newton. Fluid Mech. **151**, 69–88 10.1016/j. jnnfm.2006.12.009.
- Boger, D. V. (1987) Viscoelastic flows through contractions, Annu. Rev. Fluid Mech. 19, 157–182 10.1109/SFCS.1987.19.
- 17. Rothstein, J. P., McKinley, G. H. (1999) Extensional flow of a polystyrene Boger fluid through a 4: 1: 4 axisymmetric contraction/expansion, J. Non-Newton. Fluid Mech. 86, 61–88 10.1016/ S0377-0257(98)00202-X.
- Rothstein, J. P., McKinley, G. H. (2001) The axisymmetric contraction-expansion: the role of extensional rheology on vortex growth dynamics and the enhanced pressure drop, J. Non-Newton. Fluid Mech. 98, 33–63 10.1016/S0377-0257(01)00094-5.
- Nigen, S., Walters, K. (2002) Viscoelastic contraction flows: comparison of axisymmetric and planar configurations, J.

- Non-Newton. Fluid Mech. **102**, 343–359 /10.1016/S0377-0257(01)00186-0.
- Pérez-Camacho, M., López-Aguilar, J. E., Calderas, F., Manero, O., Webster, M. F. (2015) Pressure-drop and kinematics of viscoelastic flow through an axisymmetric contraction-expansion geometry with various contraction-ratios, J. Non-Newton. Fluid Mech. 222, 260–271 10.1016/j.jnnfm.2015.01.013
- 21. Binding, D. M., Walters, K. (1988) On the use of flow through a contraction in estimating the extensional viscosity of mobile polymer solutions, J. Non-Newton. Fluid Mech. **30**, 233–250 10.1016/0377-0257(88)85026-2.
- 22. Rothstein, J. P., Mohammadigoushki, H. (2020) Complex flows of viscoelastic wormlike micelle solutions, J. Non-Newton. Fluid Mech. **285**, 104382 10.1016/j.jnnfm.2020.104382
- Bird, R. B. (2004) Five decades of transport phenomena, AIChE J. 50, 273-287 10.1002/aic.10026.
- Denn, M. M. (2005) Fifty years of non-Newtonian Fluid Dynamics, AIChE J. 50, 2335-2345 10.1002/aic.10357.
- Walker, L. M. (2001) Rheology and structure of worm-like micelles, Curr. Opin. Colloid Interface Sci. 6, 451–456 10.1016/ S1359-0294(01)00116-9.
- Yang, J. (2002) Viscoelastic wormlike micelles and their applications, Curr. Opin. Colloid Interface Sci. 7, 276–281 10.1016/S1359-0294(02)00071-7.
- Bonn, D., Paredes, J., Denn, M. M., Berthier, L., Divoux, T., Manneville, S. (2017) Yield stress materials in soft condensed matter, Rev. Mod. Phys. 89, 035005 10.1103/RevModPhys.89.035005.
- Dreiss, C. A. (2007) Wormlike micelles: where do we stand? Recent developments, linear rheology and scattering techniques, Soft Matter 3, 956–970 10.1039/B705775J.
- 29. Dreiss, C. A. (2017) Chapter 1. Wormlike Micelles: An Introduction. In: Wormlike Micelles Advances in Systems, Characterisation and Applications, Royal Society of Chemistry, 1–8.
- Rothstein, J. P. (2008) Strong flows of viscoelastic wormlike micelle solutions, Rheology Reviews, British Society of Rheology, Aberystwyth, Wales, UK.
- Chu, Z., Dreiss, C. A., Feng, Y. (2013) Smart wormlike micelles, Chem. Soc. Rev. 42, 7174-7203 10.1039/C3CS35490C.
- Verdier, C. (2003) Rheological properties of living materials. From cells to tissues, J. Theor. Med. 5, 67-91 10.1080/10273360410001678083.
- 33. López-Aguilar, J. E., Webster, M. F., Al-Muslimawi, A. H., Tamaddon-Jahromi, H. R., Williams, P. R., Hawkins, K., Askill, C., Chin, L.C., Davies, G., Ebden, P., Lewis, K. (2015) A Computational Extensional-Rheology Study of Two Biofluid Systems, Rheol. Acta. 54, 287-305 10.1007/s00397-014-0830-y.
- 34. Tabatabaei, S., Tamaddon-Jahromi, H. R., Webster, M. F., Williams, P. R., Holder, A. J., Lewis, K. E., Davies, G.A., Griffin, L., Ebden, P., Askill, C. (2015) A CaBER computational-experimental rheological

- study on human sputum, J. Non-Newton. Fluid Mech. **222**, 272–287 10.1016/j. jnnfm.2015.03.005.
- 35. Olmsted, P. D. (2008) Perspectives on shear banding in complex fluids, Rheol. Acta. 47, 283–300 10.1007/s00397-008-0260-9.
- Horner, J. S., Armstrong, M. J., Wagner, N. J., Beris, A. N. (2019) Measurements of human blood viscoelasticity and thixotropy under steady and transient shear and constitutive modeling thereof, J. Rheol. 63, 799-813 10.1122/1.5108737.
- 37. Owens, R. G., Phillips, T. N. (2002) Computational rheology, Imperial College Press: 1st Edition.
- Walters, K., Webster, M.F. (2003) The distinctive CFD challenges of computational rheology. Int. J. Numer. Meth. Fluids. 43, 577-596 10.1002/fld.522.
- 39. Mitsoulis, E., Tsamopoulos, J. (2017) Numerical simulations of complex yieldstress fluid flows, Rheol. Acta. **56**, 1–28 10.1007/s00397-016-0981-0.
- Alves, M. A., Oliveira, P. J., Pinho, F. T. (2020) Numerical Methods for Viscoelastic Fluid Flows, Ann. Rev. Fluid Mech. 53, 509-541 10.1146/ annurev-fluid-010719-060107.
- 41. Ellero, M., Espanol P. (2018) Everything You Always Wanted to Know About S-DPD\* (\*But Were Afraid to Ask), App. Math. Mech. 39, 103-124 10.1007/s10483-018-2255-6.
- 42. Rosales-Romero, A., Vázquez-Quesada, A., Prasanna Kumar, S. S., López-Aguilar, J. E., Ellero, M. (2024) Effects of confinement-induced non-Newtonian lubrication forces on the rheology of a dense suspension, J. Non-Newton. Fluid Mech. 329, 105248 10.1016/j. jnnfm.2024.105248.
- Chilcott, M. D., Rallison, J. M. (1988) Creeping flow of dilute polymer solutions past cylinders and spheres, J. Non-Newton. Fluid Mech. 29, 381–432 10.1016/0377-0257(88)85062-6.
- 44. Rallison, J. M., Hinch, E. J. (1988). Do we understand the physics in the constitutive equation?, J. Non-Newton. Fluid Mech. 29, 37–55 10.1016/0377-0257(88)85049-3.
- Phan-Thien, N., Tanner, R. I. (1977) A new constitutive equation derived from network theory, J. Non-Newton. Fluid Mech. 2, 353-365 10.1016/0377-0257(77)80021-9.
- Larson, R. G., Wei, Y. (2019) A review of thixotropy and its rheological modelling, J. Rheol. 63, 477–501 10.1122/1.5055031.
- 47. Hommel, R. J., Graham, M. D. (2021) Constitutive modeling of dilute wormlike micelle solutions: Shear-induced structure and transient dynamics, J. Non-Newton. Fluid Mech. **295**, 104606 10.1016/j.jnnfm.2021.104606.
- 48. de Souza Mendes, P. R., Thompson R. L. (2013) A unified approach to model elasto-viscoplastic thixotropic yield-stress materials and apparent yield-stress fluids, Rheol. Acta 52, 673–694 10.1007/s00397-013-0699-1.
- 49. de Souza Mendes, P. R., Abedi, B., Thompson, R.L. (2018) Constructing a thixotropy model from rheological experiments, J. Non-Newton. Fluid Mech. 261, 1–8 10.1016/j.jnnfm.2018.08.003.

- 50. Zhou, L., McKinley G. H., Cook, L.P. (2014) Wormlike micellar solutions: III. VCM model predictions in steady and transient shearing flows, J. Non-Newton. Fluid Mech. **211**, 70–83 10.1016/j. jnnfm.2014.06.003.
- 51. Datta, S., Ardekani, A. M., Arratia, P.E., Beris, A. N., Bischofberger, I., McKinley, G. H., Eggers, J. G., López-Aguilar, J. E., Fielding, S. M., Frishman, A., Graham, M. D., Guasto, J. S., Haward, S. J., Shen, A. Q., Hormozi, S., Poole, R. J., Morozov, A., Shankar, V., Shaqfeh, E. S. G., Stark, H., Steinberg, V., Subramanian, G., Stone,
- H. A. (2022) Perspectives on viscoelastic flow instabilities and elastic turbulence, Phys. Rev. Fluids. 7, 080701 10.1103/ PhysRevFluids.7.080701.
- 52. Holenberg, Y., Lavrenteva, O. M., Shavit, U., Nir, A. (2012) Particle tracking velocimetry and particle image velocimetry study of the slow motion of rough and smooth solid spheres in a yield-stress fluid, Phys. Rev. E. 86, 066301 10.1103/ PhysRevE.86.066301.
- 53. Putz, A. M. V., Burghelea, T. I., Frigaard, I. A., Martinez, D.M. (2008) Settling of an isolated spherical particle in a yield

- stress shear thinning fluid, Phys. Fluids **20**, 033102 10.1063/1.2883937.
- 54. Tadmor, Z., Gogos, C.G. (2006) Principles of Polymer Processing, Wiley: 2nd Edition.
- Garcia-Beristain, I., Figueroa-Landeta, M., López-Aguilar, J. E., Garcia de Cortazar, M., Girot, F., Ellero, M. (2023) Numerical simulations of thixotropic semi-solid aluminium alloys in openrotor and rotor-stator mixers, J. Non-Newton. Fluid Mech. 321, 105128 10.1016/j.jnnfm.2023.105128.